

Charmonium properties in deconfinement phase in anisotropic lattice QCD

H. Iida^{1*}, T. Doi², N. Ishii³, H. Suganuma⁴ and K. Tsumura⁴

¹*Department of Physics, Tokyo Institute of Technology, Oh-okayama 2-12-1, Tokyo 152-8551, Japan*

²*RIKEN BNL Research Center, Brookhaven National Laboratory, Upton, New York 11973, USA*

³*Department of Physics, The University of Tokyo, Tokyo 113-0033, Japan and*

⁴*Department of Physics, Kyoto University, Kitashirakawaoiwake, Sakyo, Kyoto 606-8502, Japan*

(Dated: February 8, 2020)

J/Ψ and η_c above the QCD critical temperature T_c are studied in anisotropic quenched lattice QCD, considering whether the $c\bar{c}$ systems above T_c are spatially compact (quasi-)bound states or scattering states. We adopt the standard Wilson gauge action and $O(a)$ -improved Wilson quark action with renormalized anisotropy $a_s/a_t = 4.0$ at $\beta = 6.10$ on $16^3 \times (14-26)$ lattices, which correspond to the spatial lattice volume $V \equiv L^3 \simeq (1.55\text{fm})^3$ and temperatures $T \simeq (1.11-2.07)T_c$. We investigate the $c\bar{c}$ system above T_c from the temporal correlators with spatially-extended operators, where the overlap with the ground state is enhanced. To clarify whether compact charmonia survive in the deconfinement phase, we investigate spatial boundary-condition dependence of the energy of $c\bar{c}$ systems above T_c . In fact, for low-lying $c\bar{c}$ scattering states, it is expected that there appears a significant energy difference $\Delta E \equiv E(\text{APBC}) - E(\text{PBC}) \simeq 2\sqrt{m_c^2 + 3\pi^2/L^2} - 2m_c$ (m_c : charm quark mass) between periodic and anti-periodic boundary conditions on the finite-volume lattice. In contrast, for compact charmonia, there is no significant energy difference between periodic and anti-periodic boundary conditions. As a lattice QCD result, almost no spatial boundary-condition dependence is observed for the energy of the $c\bar{c}$ system in J/Ψ and η_c channels for $T \simeq (1.11-2.07)T_c$. This fact indicates that J/Ψ and η_c would survive as spatially compact $c\bar{c}$ (quasi-)bound states below $2T_c$. We also investigate a P -wave channel, χ_{c1} , at high temperature. Our results indicate that the χ_{c1} dissociate above $1.11T_c$, and there may be a spatially compact (quasi-)bound state in high-energy region, which is most probably considered to be a bound state of doubler(s). We further investigate χ_{c1} with maximally entropy method (MEM) and obtain the consistent results.

PACS numbers: 12.38.Gc, 12.38.Mh, 14.40.Gx, 25.75.Nq

I. INTRODUCTION

To complete the phase diagram of quantum chromodynamics (QCD) is one of the most challenging attempts in particle physics. The difficulty of QCD originates from the nonperturbative nature in the low-energy region, where the running coupling constant becomes large. As a consequence, color confinement and chiral symmetry breaking occur as nonperturbative phenomena, and the vacuum becomes the hadronic phase. On the other hand, at high temperature or high density region, color deconfinement and chiral symmetry restoration are expected to be realized. This phase is called the quark-gluon-plasma (QGP) phase. Actually, lattice QCD simulations show color deconfinement [1] and chiral symmetry restoration [2] above the QCD critical temperature T_c . The QGP phase transition is also investigated in various effective models [3, 4, 5, 6, 7, 8].

As an important signal of QGP creation, J/Ψ suppression [9, 10, 11, 12, 13] was theoretically proposed in the middle of 80's [4, 5]. The basic assumption of J/Ψ suppression is that J/Ψ disappears above T_c due to vanishing of the confinement potential and appearance of the Debye screening effect, which are actually shown in lattice QCD simulations [14, 15].

Experimentally, QGP search is performed at CERN-SPS and RHIC with ultra-relativistic heavy-ion collisions [9, 10, 11, 12, 13]. The experiment of NA-50 collaboration at CERN-SPS first reported the anomalous J/Ψ suppression in Pb-Pb collision (158GeV/c per nucleon) [13]. Recently, the RHIC experiments show the various signals of QGP, e.g., J/Ψ suppression [4, 5], enhancement of strange particles [16], jet quenching and high p_T suppression [17, 18], elliptic flow v_2 [17] and so on, in the collisions of Au-Au (200GeV/c per nucleon).

At first, QGP was naively speculated as simple quark-gluon gas. Nowadays, there are several indications that QGP is not simple perturbative quark-gluon gas in quenched lattice QCD. For example, it is pointed out that the spatial correlation in π and σ channels remains even in QGP phase in lattice QCD [19]. The other example is the relation between energy density and pressure, which does not satisfy the Stephan-Boltzmann relation even above T_c [14]. The calculation of transport coefficients at finite temperature on quenched lattices also shows the strongly correlated gluon plasma [20]. These simulations indicate that some of the nonperturbative properties may survive in QGP phase. Experimentally, in the reports of RHIC [9, 10, 11, 12], QGP seems to behave as perfect liquid, which strongly interacts, rather than dilute gas, from the comparison of the experiments with numerical simulations of hydrodynamics [21]. The strongly correlated deconfined phase is called strongly coupled QGP (sQGP) phase, and is investigated with

*E-mail: iida@th.phys.titech.ac.jp

much attention.

Very recently, some lattice QCD calculations indicate an interesting possibility that J/Ψ and η_c seem to survive even above T_c [22, 23, 24, 25]. In Ref. [22], the authors calculate correlators of charmonia at finite temperature and find the strong spatial correlation between c and \bar{c} even above T_c . In Refs. [23, 24, 25], the authors extract spectral functions of charmonia from temporal correlators at high temperature using the maximally entropy method (MEM). Although there are some quantitative differences, the peaks corresponding to J/Ψ and η_c seem to survive even above T_c ($T_c < T < 2T_c$) in the $c\bar{c}$ spectral function.

However, all of these calculations may suffer from a possible problem that the observed $c\bar{c}$ state on lattices is not a nontrivial charmonium but a trivial $c\bar{c}$ scattering state, because it is difficult to distinguish these two states in lattice QCD. One of the reasons of the difficulty is that a narrow peak does not immediately indicate a spatially compact (quasi-)bound state. In QGP phase, the potential between q and \bar{q} is considered to be the Yukawa potential due to the Debye screening [14]. Therefore, the binding energy of q and \bar{q} above T_c may be small. Then, the bound state of q and \bar{q} may not be spatially compact. In addition, MEM has a relatively large error, which sometimes leads to uncertainty for the structure of the spectral function.

In this paper and our previous proceeding [26], using lattice QCD, we aim to clarify whether the $c\bar{c}$ system above T_c is a spatially compact (quasi-)bound state or a scattering state, which is spatially spread. To distinguish these two states, we investigate spatial boundary-condition dependence of the energy of the $c\bar{c}$ system by comparing results on periodic and anti-periodic boundary conditions. If the $c\bar{c}$ system is a scattering state, there appears an energy difference ΔE between the two boundary conditions as $\Delta E \simeq 2\sqrt{m_c^2 + 3\pi^2/L^2} - 2m_c$ with the charm quark mass m_c on a finite-volume lattice with L^3 (see Sec. II). If the $c\bar{c}$ system is a spatially compact (quasi-)bound state, the boundary-condition dependence is expected to be small even in finite volume. In Ref. [27], by changing the spatial periodicity of (anti-)quarks, the authors actually try to distinguish between a scattering state and a spatially compact resonance.

In this study, we use anisotropic lattice QCD with anisotropy $a_s/a_t = 4.0$. The reason why we use the anisotropic lattice is as follows. At finite temperature T , the temporal lattice size is restricted to $0 \leq t \leq 1/T$. Then, in calculating the temporal correlator $G(t)$ at high temperature, we cannot take the sufficient number of points for $G(t)$. By using anisotropic lattice, more data points are available for $G(t)$. For the accurate measurement of $G(t)$, we use such a technical improvement of lattice QCD.

For further technical improvement, we use spatially-extended operators with hadron size in the actual lattice calculations at high temperature. We are interested in the low-lying spectrum in the $c\bar{c}$ systems at high temper-

ature in this study, since the ground-state component is desired to dominate in the range of $0 \leq t \leq 1/T$. For this purpose, we use the spatially-extended operator to enhance the ground-state overlap.

This paper is organized as follows. In Sec. II, we discuss the method to distinguish a spatially compact (quasi-)bound state from a scattering state by changing the spatial boundary condition for (anti-)quarks. In Sec. III, we briefly explain anisotropic lattice QCD. In Sec. IV, we show the method to extract the energy of the ground state of $c\bar{c}$ systems from temporal correlators at finite temperature in lattice QCD. Section V shows lattice QCD results of J/Ψ and η_c above T_c . Using the method discussed in Sec. II, we find the survival of J/Ψ and η_c as spatially compact (quasi-)bound states above T_c ($\sim 2T_c$). In Sec. VI, we show the analysis of a P -wave state corresponding to χ_{c1} above T_c , and find that χ_{c1} already dissolves into the $c\bar{c}$ scattering state at $1.11T_c$. Section VII is devoted to conclusion and outlook.

II. METHOD TO DISTINGUISH COMPACT STATES FROM SCATTERING STATES

In this section, we explain the method to distinguish compact states from scattering states in term of their spatial extension.

For this purpose, we investigate the $c\bar{c}$ system on the periodic boundary condition (PBC) and on the anti-periodic boundary condition (APBC), respectively, and examine spatial boundary-condition dependence for the $c\bar{c}$ system. Here, on the PBC and the APBC case, we impose periodic and anti-periodic boundary condition for (anti-)quarks on a finite-volume lattice, respectively.

For a compact $c\bar{c}$ (quasi-)bound state, the wave function of the $c\bar{c}$ system is spatially localized and insensitive to spatial boundary conditions in lattice QCD as shown in Fig. 1(b), so that the charmonium behaves as a compact boson and its energy on APBC is almost the same as that on PBC [27].

For a $c\bar{c}$ scattering state, the wave function is spatially spread and sensitive to spatial boundary conditions as shown in Fig. 1(b) and hence there emerges the energy difference between PBC and APBC due to the non-zero relative momentum of c and \bar{c} on APBC even in the lowest energy state. On PBC, the momentum of a quark or an anti-quark is discretized as

$$p_k = \frac{2n_k\pi}{L} \quad (k = 1, 2, 3, n_k \in \mathbf{Z}) \quad (1)$$

on the finite lattice with the spatial volume L^3 . Therefore, on PBC, the minimum momentum is $\vec{p}_{\min} = \vec{0}$. On APBC, the (anti-)quark momentum is discretized as

$$p_k = \frac{(2n_k + 1)\pi}{L} \quad (k = 1, 2, 3, n_k \in \mathbf{Z}). \quad (2)$$

In this case, the (anti-)quark momentum cannot take zero even in the lowest energy state. Then, the minimum

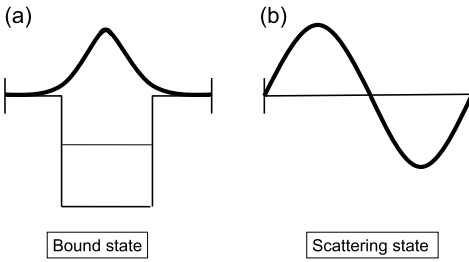


FIG. 1: Schematic figures for boundary-condition dependence of a bound state (a) and a scattering state (b). The wave function of a bound state is spatially localized, and that of scattering state spatially spreads. Therefore, the bound state is insensitive to spatial boundary condition, while the scattering state is sensitive to spatial boundary condition in a finite-size box.

(anti-)quark momentum is

$$|\vec{p}_{\min}| = \frac{\sqrt{3}\pi}{L}, \quad (3)$$

as is depicted in Fig. 2. Thus, there is an energy difference between PBC and APBC for the lowest $c\bar{c}$ scattering state. Neglecting the interaction between c and \bar{c} , the energy difference is estimated as

$$\begin{aligned} \Delta E &\simeq 2\sqrt{m_c^2 + \vec{p}_{\min}^2} - 2m_c \\ &= 2\sqrt{m_c^2 + 3\pi^2/L^2} - 2m_c, \end{aligned} \quad (4)$$

where m_c is charm quark mass. The minimum momentum of a quark and an anti-quark in the case of scattering state is depicted in Fig. 2.

Table I summarizes the mass of the $c\bar{c}$ compact bound state (charmonia) and the energy of the $c\bar{c}$ scattering state both on PBC and APBC. In the case of the $c\bar{c}$ scattering state, there emerges the energy difference between PBC and APBC.

Such a method, to distinguish a compact (quasi-)bound state from a scattering state by changing boundary conditions, is actually used in Ref. [27]. This method is essentially based on the finiteness of lattice volume. Note that the finite volume is used in several studies for the analyses of a scattering state and/or a compact bound state in lattice QCD [28, 29, 30].

III. ANISOTROPIC LATTICE QCD

In this paper, we adopt anisotropic lattice QCD for the study of high-temperature QCD, as was mentioned in Sec. I. We explain anisotropic lattice QCD in the following.

For the gauge field, we adopt the standard plaquette action on an anisotropic lattice as [27, 31]

$$\begin{aligned} S_G &= \frac{\beta}{N_c} \frac{1}{\gamma_G} \sum_{s,i < j \leq 3} \text{ReTr}\{1 - P_{ij}(s)\} \\ &+ \frac{\beta}{N_c} \gamma_G \sum_{s,i \leq 3} \text{ReTr}\{1 - P_{i4}(s)\}, \end{aligned} \quad (5)$$

where $P_{\mu\nu}$ denotes the plaquette operator. In the simulation, we take $\beta \equiv 2N_c/g^2 = 6.10$ and the bare anisotropy $\gamma_G = 3.2103$, which lead to the renormalized anisotropy as $a_s/a_t = 4.0$. The scale is set by the Sommer scale as $r_0^{-1} = 395\text{MeV}$. Then, the spatial and the temporal lattice spacing are evaluated as $a_s^{-1} \simeq 2.03\text{GeV}$ (i.e., $a_s \simeq 0.097\text{fm}$), and $a_t^{-1} \simeq 8.12\text{GeV}$ (i.e., $a_t \simeq 0.024\text{fm}$), respectively. The adopted lattice sizes are $16^3 \times (14 - 26)$, which correspond to the spatial lattice size as $L \simeq 1.55\text{fm}$ and the temperature as $(1.11 - 2.07)T_c$. Here, the critical temperature is estimated as $T_c = (260 - 280)\text{MeV}$ at the quenched level [32]. We use 999 gauge configurations, which are picked up every 500 sweeps after the thermalization of 20,000 sweeps. We adopt the jackknife error estimate for lattice data.

For quarks, we use $O(a)$ -improved Wilson (clover) action on the anisotropic lattice as [27, 31]

$$\begin{aligned} S_F &\equiv \sum_{x,y} \bar{\psi}(x)K(x,y)\psi(y), \\ K(x,y) &\equiv \\ &\delta_{x,y}\kappa_t\{(1 - \gamma_4)U_4(x)\delta_{x+4,y} + (1 + \gamma_4)U_4^\dagger(x - \hat{4})\delta_{x-4,y}\} \\ &- \kappa_s \sum_i \{(r - \gamma_i)U_i(x)\delta_{x+\hat{i},y} + (r + \gamma_i)U_i^\dagger(x - \hat{i})\delta_{x-\hat{i},y}\} \\ &- \kappa_s c_E \sum_i \sigma_{i4}F_{i4}\delta_{x,y} - r\kappa_s c_B \sum_{i < j} \sigma_{ij}F_{ij}\delta_{x,y}, \end{aligned} \quad (6)$$

which is anisotropic version of the Fermilab action [33]. κ_s and κ_t denote the spatial and the temporal hopping parameters, respectively, and r the Wilson parameter. c_E and c_B are the clover coefficients. The tadpole improvement is done by the replacement of $U_i(x) \rightarrow U_i(x)/u_s$, $U_4(x) \rightarrow U_4(x)/u_t$, where u_s and u_t are the mean-field values of the spatial and the temporal link variables, respectively. The parameters $\kappa_s, \kappa_t, r, c_E, c_B$ are to be tuned so as to keep the Lorentz symmetry up to $O(a^2)$. At the tadpole-improved tree-level, this requirement leads to $r = a_t/a_s$, $c_E = 1/(u_s u_t^2)$, $c_B = 1/u_s^3$ and the tuned fermionic anisotropy $\gamma_F \equiv (u_t \kappa_t)/(u_s \kappa_s) = a_s/a_t$. For the charm quark, we take $\kappa = 0.112$ with $1/\kappa \equiv 1/(u_s \kappa_s) - 2(\gamma_F + 3r - 4)$, which corresponds to the hopping parameter in the isotropic lattice. The bare quark mass m_0 in spatial lattice unit is expressed as $m_0 = \frac{1}{2}(\frac{1}{\kappa} - 8)$. We summarize the lattice parameters and related quantities in Table II. With the present lattice QCD setup, the masses of J/Ψ , η_c and χ_{c1} are calculated as $m_{J/\Psi} \simeq 3.07\text{GeV}$, $m_{\eta_c} \simeq 2.99\text{GeV}$ and $m_{\chi_{c1}} \simeq 3.57\text{GeV}$ at $T \simeq 0$. These values almost the

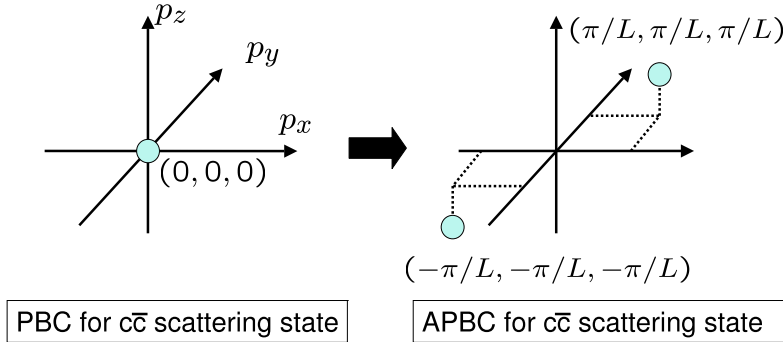


FIG. 2: Pictorial expression of minimum momentum of the (anti-)quark on PBC and APBC in the case of $c\bar{c}$ scattering state in the center of mass frame. c and \bar{c} are in the finite-size with the spatial volume L^3 . On PBC, both particles have zero lowest momentum in the lowest state. On the other hand, on APBC, quark and anti-quark have an opposite non-zero momentum.

TABLE I: Summary of the boundary-condition dependence of the compact charmonia and the $c\bar{c}$ scattering state. The energy difference ΔE is calculated on the spatial lattice size $L = 1.55\text{fm}$ and the charm quark mass $m_c \simeq 1.3\text{GeV}$.

charmonia	$c\bar{c}$ scattering state
mass (energy) on PBC	bound state mass M
mass (energy) on APBC	bound state mass M
$\Delta E \equiv E(\text{APBC}) - E(\text{PBC})$	$\simeq 0$
$\simeq 2m_c$	$\simeq 2\sqrt{m_c^2 + \vec{p}_{\min}^2}$
$\simeq 2\sqrt{m_c^2 + \vec{p}_{\min}^2} - 2m_c \simeq 0.35\text{GeV}$	

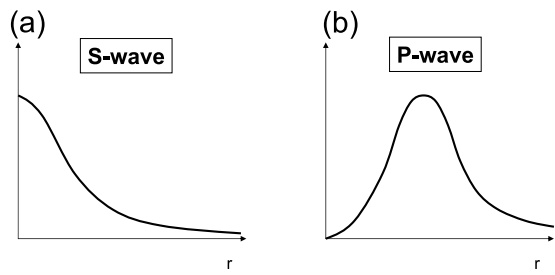


FIG. 3: Schematic figure for radial wave functions of $c\bar{c}$ compact bound states for the S -wave state (a) and the P -wave state (b). The S -wave state can be approximated with a Gaussian form $e^{-r^2/2\rho^2}$. In contrast, the wave-function of P -wave state should be zero at $r = 0$ and spatially spreads due to the centrifugal potential.

same as the experimental ones, $m_{J/\Psi}(\text{exp}) = 3.10\text{GeV}$, $m_{\eta_c}(\text{exp}) = 2.98\text{GeV}$ and $m_{\chi_{c1}}(\text{exp}) = 3.51\text{GeV}$.

IV. TEMPORAL CORRELATORS OF $c\bar{c}$ SYSTEMS AT FINITE TEMPERATURE ON ANISOTROPIC LATTICE

To investigate the low-lying state at high temperature from the temporal correlator, it is practically desired to use a “good” operator with a large overlap with ground state (ground-state overlap), due to limitation of the temporal lattice size. To this end, we use a spatially-extended

operator of the Gaussian type as

$$O(t, \vec{x}) \equiv N \sum_{\vec{y}} \exp \left\{ -\frac{|\vec{y}|^2}{2\rho^2} \right\} \bar{c}(t, \vec{x} + \vec{y}) \Gamma c(t, \vec{x}) \quad (7)$$

with the extension radius ρ as the hadronic size in the Coulomb gauge [27, 31]. N is a normalization constant. $\Gamma = \gamma_k$ ($k = 1, 2, 3$) and $\Gamma = \gamma_5$ correspond to $1^-(J/\Psi)$ and $0^-(\eta_c)$ channels, respectively. Note here that this form (7) is suitable for S -wave states (see Fig. 3(a)). In the actual calculation, the size parameter ρ is optimally chosen in terms of the ground-state overlap. The energy of the low-lying state is calculated from the temporal correlator,

$$G(t) \equiv \frac{1}{V} \sum_{\vec{x}} \langle O(t, \vec{x}) O^\dagger(0, \vec{0}) \rangle, \quad (8)$$

where the total spatial momentum of the $c\bar{c}$ system is projected to be zero.

In accordance with the temporal periodicity at finite temperature, we define the effective mass $m_{\text{eff}}(t)$ from the correlator $G(t)$ by the cosh-type function as [32]

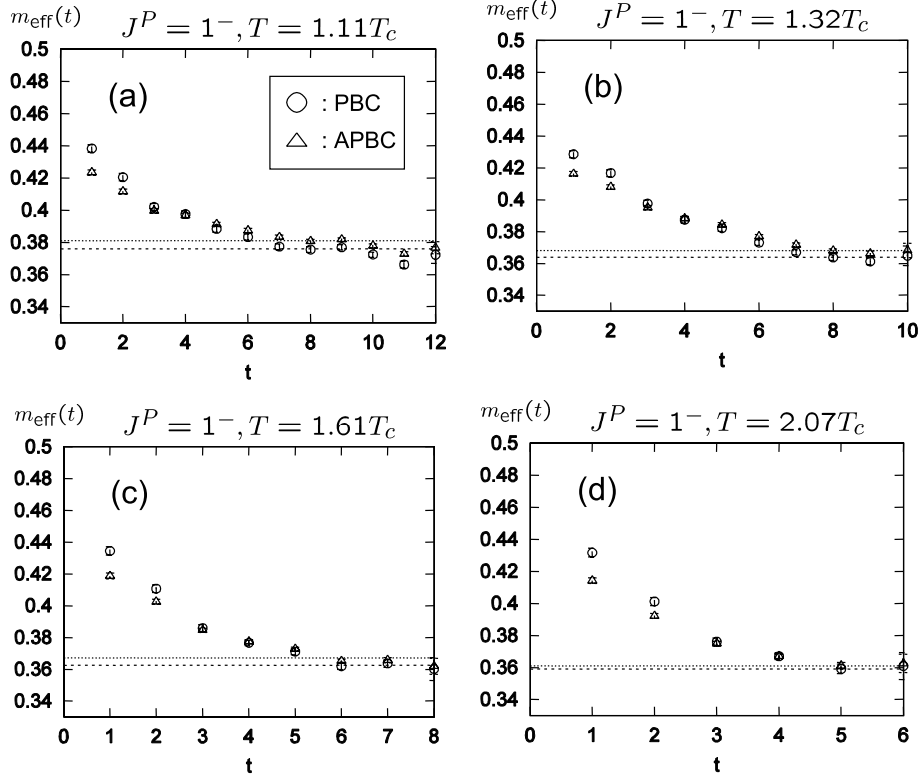
$$\frac{G(t)}{G(t+1)} = \frac{\cosh[m_{\text{eff}}(t)(t - N_t/2)]}{\cosh[m_{\text{eff}}(t)(t + 1 - N_t/2)]} \quad (9)$$

with the temporal lattice size N_t . If the correlator $G(t)$ is saturated by the lowest level, it behaves as

$$G(t) \simeq A \cosh \left[m_0(t - \frac{N_t}{2}) \right], \quad (10)$$

TABLE II: Lattice parameters and related quantities in our anisotropic lattice QCD calculation.

β	lattice size	a_s^{-1}	a_t^{-1}	γ_G	u_s	u_t	γ_F	κ
6.10	$16^3 \times (14 - 26)$	2.03GeV	8.12GeV	3.2103	0.8059	0.9901	4.0	0.112

FIG. 4: Effective masses of J/Ψ at $1.11T_c$ (a), $1.32T_c$ (b), $1.61T_c$ (c) and $2.07T_c$ (d) in the lattice unit with $a_t = (8.12\text{GeV})^{-1}$. The circles and the triangles denote the results on PBC and APBC, respectively. The dashed and dotted lines denote $E(\text{PBC})$ and $E(\text{APBC})$ obtained from the best-fit analysis, respectively.

where m_0 is the energy of the lowest state. In this case, the solution $m_{\text{eff}}(t)$ in Eq. (9) coincides with the lowest-state energy m_0 in Eq. (10).

To find the optimal value of the extension radius ρ , we set two criterions. First, an effective mass $m_{\text{eff}}(t)$ of a temporal correlator $G(t)$ with ρ should have plateau region in terms of t . Second, the ground-state component should be large enough in the plateau region of $m_{\text{eff}}(t)$. For the estimation of the ground state overlap, we define $g_{\text{fit}}(t)$ as [32]

$$g_{\text{fit}}(t) \equiv A' \cosh[m'(t - N_t/2)], \quad (11)$$

where A' and m' are determined by fitting $g_{\text{fit}}(t)$ to $G(t)/G(0)$ in the plateau region. In general, $g_{\text{fit}}(0) \leq 1$ is satisfied, and $g_{\text{fit}}(0) = 1$ is achieved if and only if $G(t)$ is completely dominated by the ground-state contribution in the whole region of $0 \leq t \leq 1/T$. Therefore, we use $g_{\text{fit}}(0)$ as an index of the ground-state overlap. Namely, if $g_{\text{fit}}(0)$ with ρ_1 is larger than that with ρ_2 , we regard the operator with ρ_1 as a better operator which

has larger ground-state overlap than that with ρ_2 . Under these criterions, we determine the optimal operator in the range of $\rho = 0$ (0.1fm) 0.5fm. For $\rho = 0$ and 0.1fm, the effective masses are found to have no plateau region. Accordingly, we abandon these extension radii. Next, we examine $g_{\text{fit}}(0)$ for $\rho = (0.2 - 0.5)$ fm, and find that the optimal size of ρ is $\rho = (0.2 - 0.3)$ fm at all temperatures for $c\bar{c}$ systems. Actually, the results of $\rho = 0.2$ fm and 0.3fm are almost the same. Hereafter, we show the numerical results for $\rho = 0.2$ fm.

V. LATTICE QCD RESULTS FOR J/Ψ AND η_c CHANNELS ABOVE T_c

We investigate the $c\bar{c}$ systems above T_c both in $J/\Psi(J^P = 1^-)$ and $\eta_c(J^P = 0^-)$ channels in lattice QCD. For each channel, we calculate the temporal correlator $G(t)$ following Eq. (8), where the total spatial momentum is projected to be zero. From $G(t)$, we extract

TABLE III: The energy of the $c\bar{c}$ system in the J/Ψ channel ($J^P = 1^-$) on PBC and APBC at $\beta = 6.10$ and $\rho = 0.2\text{fm}$ at each temperature. The statistical errors are smaller than 0.01GeV . We list also uncorrelated χ^2/N_{DF} and $\Delta E \equiv E(\text{APBC}) - E(\text{PBC})$.

temperature	fit range	$E(\text{PBC})$ [χ^2/N_{DF}]	$E(\text{APBC})$ [χ^2/N_{DF}]	ΔE
$1.11T_c$	7–11	3.05GeV [0.14]	3.09GeV [0.61]	0.04GeV
$1.32T_c$	8–11	2.95GeV [0.34]	2.98GeV [0.33]	0.03GeV
$1.61T_c$	6–9	2.94GeV [0.10]	2.98GeV [0.22]	0.04GeV
$2.07T_c$	5–7	2.91GeV [0.03]	2.93GeV [0.04]	0.02GeV

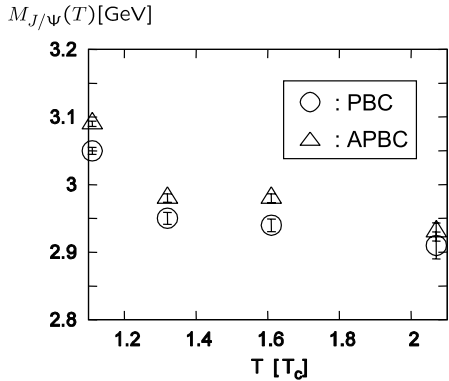


FIG. 5: Temperature dependence of the pole mass (energy) $M_{J/\Psi}(T)$ of J/Ψ for $(1.11 - 2.07)T_c$ on PBC (circles) and APBC (triangles). The circles and the triangles correspond to $E(\text{PBC})$ and $E(\text{APBC})$ of the $c\bar{c}$ system, respectively. The energy difference $\Delta E \equiv E(\text{APBC}) - E(\text{PBC}) \simeq (0.02 - 0.04)\text{GeV}$ between PBC and APBC are considerably smaller than that of $c\bar{c}$ scattering state, $\Delta E \simeq 0.35\text{GeV}$.

the effective mass $m_{\text{eff}}(t)$ both on PBC and APBC, and examine their spatial boundary-condition dependence. From the cosh-type fit for the correlator $G(t)$ in the plateau region of effective mass $m_{\text{eff}}(t)$, we extract the energies, $E(\text{PBC})$ and $E(\text{APBC})$, of the low-lying $c\bar{c}$ system on PBC and APBC, respectively. In fact, if the $c\bar{c}$ system is a spatially compact bound state, one can expect $E(\text{PBC}) \simeq E(\text{APBC})$, which coincides with the bound state mass. On the other hand, if the $c\bar{c}$ system is a scattering state, $E(\text{PBC})$ and $E(\text{APBC})$ are expected to be the corresponding thresholds of the $c\bar{c}$ scattering state, i.e., $E(\text{PBC}) \simeq 2m_c$ and $E(\text{APBC}) \simeq 2\sqrt{m_c^2 + \vec{p}_{\text{min}}^2}$.

Figure 4 shows effective-mass plots of J/Ψ on PBC and APBC for $(1.11 - 2.07)T_c$ in lattice QCD. Table III shows the boundary-condition dependence of the energy of the $c\bar{c}$ system in the J/Ψ channel for $(1.11 - 2.07)T_c$. It is remarkable that almost no spatial boundary-condition dependence is found for the low-lying energy of the $c\bar{c}$ system, i.e., $\Delta E \equiv E(\text{APBC}) - E(\text{PBC}) \simeq 0$. This contrasts to the $c\bar{c}$ scattering case of $\Delta E \simeq 2\sqrt{m_c^2 + 3\pi^2/L^2} - 2m_c \simeq 0.35\text{GeV}$ for $L \simeq 1.55\text{fm}$ and $m_c \simeq 1.3\text{GeV}$ as was discussed in Sec. II. This result indicates that J/Ψ survives for $(1.11 - 2.07)T_c$ as spatially compact (quasi-)bound state. Figure 5 shows the temperature dependence of the pole mass of J/Ψ , $M_{J/\Psi}(T)$.

Figure 6 shows effective mass plots of η_c on PBC and APBC for $(1.11 - 2.07)T_c$. Table IV summarizes the $c\bar{c}$ system in the η_c channel on PBC and APBC at each temperature. Again, almost no spatial boundary-condition dependence is found as $\Delta E \equiv E(\text{APBC}) - E(\text{PBC}) \simeq 0$. This result indicates that η_c also survives for $(1.11 - 2.07)T_c$ as spatially compact (quasi-)bound state. Figure 7 shows the temperature dependence of the pole mass of η_c , $M_{\eta_c}(T)$.

From Figs. 4 and 6, one finds that $m_{\text{eff}}(t)$ on APBC is saturated by the low-lying state more rapidly than that on PBC, i.e., $m_{\text{eff}}^{\text{PBC}}(t) > m_{\text{eff}}^{\text{APBC}}(t)$ for small t and $m_{\text{eff}}^{\text{PBC}}(t) \simeq m_{\text{eff}}^{\text{APBC}}(t)$ for large t . This fact may be explained as follows. In the channels of J/Ψ and η_c , there are scattering states in addition to the bound state. On APBC, the low-lying scattering states are shifted to higher energy region in contrast to the compact bound state. Thus, the contributions of scattering states dump rapidly on APBC. The (slight) smallness of errorbars on APBC compared with those on PBC may be explained by the same reason (see Figs. 5 and 7).

In Fig. 8, we compare $M_{J/\Psi}(T)$ with $M_{\eta_c}(T)$ on PBC. It is interesting that there occurs the inversion of $M_{J/\Psi}(T)$ and $M_{\eta_c}(T)$ above $1.3T_c$. In fact, $M_{J/\Psi}(T)$ decreases as temperature increases, while $M_{\eta_c}(T)$ is almost unchanged (see Fig. 5 and 7). We observe the significant reduction of $M_{J/\Psi}(T)$ of the order of 100MeV . (We note that thermal width broadening also leads to the same effect of the pole-mass reduction [32].) In any case, it would be interesting to investigate the possible change of the J/Ψ mass above T_c .

VI. LATTICE QCD RESULTS FOR χ_{c1} CHANNEL ABOVE T_c

We also perform the analysis in axial vector $\chi_{c1}(J^P = 1^+)$ channel above T_c in lattice QCD. χ_{c1} is a P -wave $c\bar{c}$ meson and its wave function tends to spread due to the centrifugal potential $l(l+1)/m_c r^2$ (r : relative distance between c and \bar{c} , l : orbital angular momentum) compared with S -wave states such as J/Ψ and η_c (see Fig. 3). According to this spread wave function, χ_{c1} is expected to be sensitive to vanishing of linear potential and Debye screening effect above T_c . In fact, the dissociation temperature of χ_{c1} would be lower than that of J/Ψ and η_c . Thus, we study the P -wave $c\bar{c}$ meson χ_{c1}

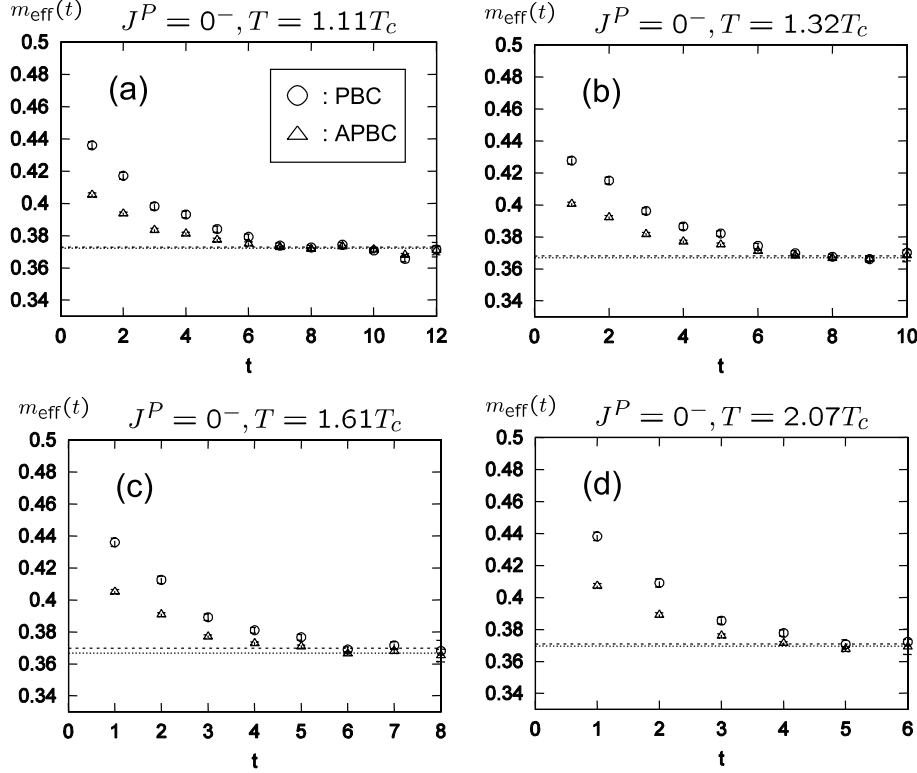


FIG. 6: Effective masses of η_c at $1.11T_c$ (a), $1.32T_c$ (b), $1.61T_c$ (c) and $2.07T_c$ (d) in the lattice unit with $a_t \simeq (8.12\text{GeV})^{-1}$. The circles and the triangles denote the results on PBC and APBC, respectively. The dashed and the dotted lines denote $E(\text{PBC})$ and $E(\text{APBC})$ obtained from the best-fit analysis, respectively.

TABLE IV: The energy of the $c\bar{c}$ system in the η_c channel ($J^P = 0^-$) on PBC and APBC at $\beta = 6.10$ and $\rho = 0.2\text{fm}$ at each temperature. The statistical errors are smaller than 0.01GeV . We list also uncorrelated χ^2/N_{DF} and $\Delta E \equiv E(\text{APBC}) - E(\text{PBC})$.

temperature	fit range	$E(\text{PBC})$ [χ^2/N_{DF}]	$E(\text{APBC})$ [χ^2/N_{DF}]	ΔE
$1.11T_c$	7–11	3.03GeV [0.04]	3.02GeV [0.17]	-0.01GeV
$1.32T_c$	7–11	2.99GeV [0.78]	2.98GeV [0.82]	-0.01GeV
$1.61T_c$	6–9	3.00GeV [0.31]	2.97GeV [0.38]	-0.03GeV
$2.07T_c$	5–7	3.01GeV [0.03]	3.00GeV [0.07]	-0.01GeV

at finite temperature in lattice QCD. For the calculation in χ_{c1} channel, we use the spatially-extended operator of Eq. (7) with $\Gamma = \gamma_5\gamma_k$ and various sizes. The parameters of lattice QCD are the same as those in the calculation of J/Ψ and η_c in the previous section.

Figure 9 shows the effective-mass plot in χ_{c1} channel at $1.11T_c$ with the size parameter $\rho = 0.2\text{fm}$. There are two remarkable features. First, the spatial boundary-condition dependence of the energy can be observed, and the energy difference between PBC and APBC is significant and is the order of 0.4GeV . This energy difference can be interpreted as the $c\bar{c}$ scattering state with $m_c \simeq 1\text{GeV}$. Second, the effective mass is located around 2GeV for large t region. In fact, the ground state in χ_{c1} channel is estimated as around 2GeV . This ground state energy seems to coincide with the $c\bar{c}$ thresh-

old value, which is much smaller than the χ_{c1} mass, $m_{\chi_{c1}} \simeq 3.5\text{GeV}$. This fact shows that χ_{c1} vanishes already at $1.11T_c$, and the lowest state is just a scattering state of $c\bar{c}$ at $1.11T_c$ in the χ_{c1} channel.

Next, we perform lattice QCD search for a possible (quasi-)bound state corresponding to χ_{c1} around 3.5GeV above T_c . Because χ_{c1} is a P -wave state, the wave function of χ_{c1} is not spherical. Moreover, its radial wave function should be zero at the origin due to the centrifugal potential, as shown in Fig. 3(b). Therefore, the spherical and Gaussian type extension of an operator, which is suitable for a S -wave state (see Fig. 3(a)), may not be a good choice to investigate a possible P -wave bound state of χ_{c1} . Therefore, in the following, we show the calculations with local (non-extended) operator.

Figure 10 shows the effective-mass plot of χ_{c1} chan-

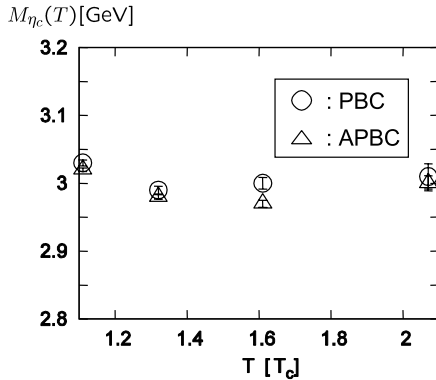


FIG. 7: Temperature dependence of the pole mass (energy) $M_{\eta_c}(T)$ of η_c for $(1.11 - 2.07)T_c$ on PBC (circles) and APBC (triangles). The energy difference $\Delta E \simeq 0$ between PBC and APBC are also considerably smaller than that of $c\bar{c}$ scattering state as well as J/Ψ case.

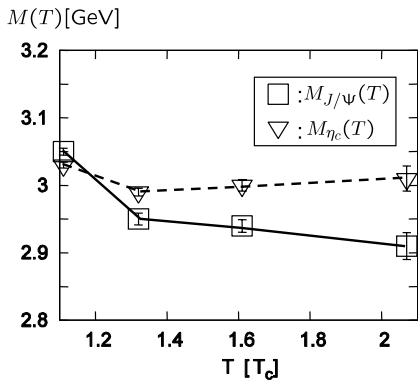


FIG. 8: Temperature dependence of the pole mass (on PBC) of J/Ψ and η_c for $(1.11 - 2.07)T_c$. The squares denote $M_{J/\Psi}(T)$ and the inverse triangles denote $M_{\eta_c}(T)$. There occurs the level inversion of J/Ψ and η_c above $1.3T_c$.

nel with local operator at $1.11T_c$. The effective mass is located around 4.5GeV for large t , which is much larger than the mass of χ_{c1} , $m_{\chi_{c1}} \simeq 3.5\text{GeV}$. Thus, also χ_{c1} cannot be observed in the calculation with local operator, again. Here, we consider the “observed” state around 4.5GeV at $1.11T_c$ in lattice QCD. If the state is assumed to be a scattering state of two particles which have the mass $m = 4.5\text{GeV}/2 \simeq 2\text{GeV}$, then the energy difference between PBC and APBC is expected to be $\Delta E \simeq 0.24\text{GeV}$. However, the observed energy difference is much smaller than that of the scattering state. This fact may indicate a possibility that the observed state around 4.5GeV is a spatially compact bound state, instead of a scattering state.

For further analysis of χ_{c1} above T_c , we perform the analysis of χ_{c1} with maximally entropy method (MEM) [23, 24, 25]. Using MEM, we can extract the spectral function $A(\omega)$ from the temporal correlator $G(t)$, where the relation between $A(\omega)$ and $G(t)$ at finite temperature

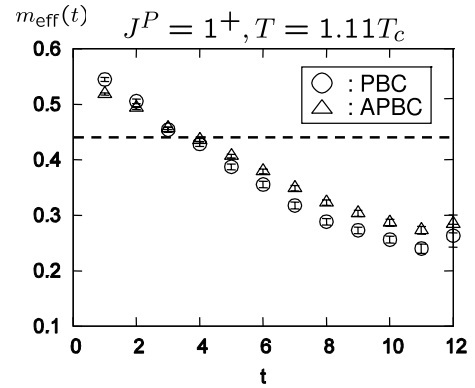


FIG. 9: Effective mass of χ_{c1} channel at $1.11T_c$ with spatially extended operator for $\rho = 0.2\text{fm}$ in the lattice unit with $a_t = (8.12\text{GeV})^{-1}$. The circles and the triangles denote the results on PBC and APBC, respectively. A significant energy difference of the order of 0.4GeV is found between PBC and APBC for large t . The dashed line denotes the mass of χ_{c1} , $m_{\chi_{c1}} = 3.51\text{GeV}$ (exp.), at zero temperature.

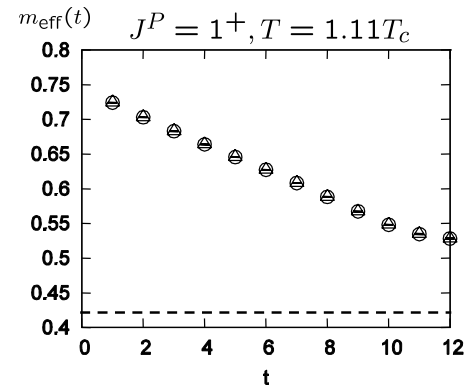


FIG. 10: Effective mass of χ_{c1} channel at $1.11T_c$ with local operator in the lattice unit with $a_t = (8.12\text{GeV})^{-1}$. The circles and the triangles denote the results on PBC and APBC, respectively. The dashed line denotes the mass of χ_{c1} , $m_{\chi_{c1}} = 3.51\text{GeV}$ (exp.), at zero temperature.

T is given by

$$G(t) = \int_0^\infty d\omega K(t, \omega) A(\omega),$$

$$K(t, \omega) = (e^{-t\omega} + e^{-(1/T-t)\omega})/(1 - e^{-\omega/T}). \quad (12)$$

We use the Wilson quark action in the calculation of lattice QCD data for MEM. Instead of the improvement of the action, we use the finer lattice spacing $a_t = a_s/4 = (20.2\text{GeV})^{-1} = 9.75 \times 10^{-3}\text{fm}$ with $\beta = 7.0$. The lattice size is $20^3 \times 46$, which corresponds to the lattice volume $L^3 \simeq (0.78\text{fm})^3$ and the temperature $T = 1.62T_c$.

Figure 11(a) shows the spectral function in χ_{c1} ($J^P = 1^+$) channel on PBC at $1.62T_c$. There is no peak which corresponds to χ_{c1} ($m_{\chi_{c1}} \simeq 3.5\text{GeV}$). In the high-energy region around 6GeV , we can see the sharp peak in the spectral function. Figure 11(b) shows the spectral function in χ_{c1} channel on APBC at $1.62T_c$. There is almost

no difference between PBC and APBC. From Fig. 11(c), we can confirm that the spectral function on PBC almost coincides with that on APBC. This fact indicates that the peak around 6GeV corresponds to a spatially compact (quasi-)bound state. Thus, the MEM analysis also shows the consistent conclusion: dissociation of χ_{c1} occurs already at $1.62T_c$, and there is a compact bound state at high-energy region. However, the bound state mass ($\simeq 6$ GeV) is largely different from 4.5GeV in the previous analysis according to the calculation of the different β . This difference may be explained by regarding this state as a bound state of doubler(s) [25, 34]. (Here, we note that the appearance of the peak structure is highly nontrivial, because the default function of MEM is a perturbative one, which does not have the peak structure.) The further analysis of charmonia at high temperature with MEM will be reported in Ref. [35].

VII. CONCLUSION AND OUTLOOK

We have investigated J/Ψ and η_c above T_c with anisotropic quenched lattice QCD to clarify whether the $c\bar{c}$ systems above T_c are compact (quasi-)bound states or scattering states. We have adopted the standard Wilson gauge action and the $O(a)$ -improved Wilson quark action with renormalized anisotropy $a_s/a_t = 4.0$. We have used $\beta = 6.10$ on $16^3 \times (14 - 26)$ lattices, which correspond to the spatial lattice volume $V \equiv L^3 \simeq (1.55\text{fm})^3$ and $T = (1.11 - 2.07)T_c$. To clarify whether compact charmonia survive in the deconfinement phase, we have investigated spatial boundary-condition dependence of the energy of $c\bar{c}$ systems above T_c . In fact, for low-lying $c\bar{c}$ scattering states, it is expected that there appears a significant energy difference $\Delta E \equiv E(\text{APBC}) - E(\text{PBC})$ between periodic and anti-periodic boundary conditions as $\Delta E \simeq 2\sqrt{m_c^2 + 3\pi^2/L^2} - 2m_c$ on the finite-volume lattice. For enhancement of the ground-state overlap, we have used the spatially extended operator with Gaussian function.

As a result, both in J/Ψ and η_c channels, we have found almost no spatial boundary-condition dependence of the energy of the low-lying $c\bar{c}$ system even on the finite-volume lattice for $(1.11 - 2.07)T_c$. These results indicate that J/Ψ and η_c survive as spatially compact $c\bar{c}$ (quasi-) bound states for $(1.11 - 2.07)T_c$. Also, the inversion of levels of J/Ψ and η_c above $1.3T_c$ has been seen. In fact, we have observed the significant reduction of the J/Ψ pole mass of about 100MeV, above $1.3T_c$. Experimentally, it may be interesting to investigate the possible change of the J/Ψ mass above T_c .

We have also calculated the $c\bar{c}$ system in χ_{c1} channel above T_c in lattice QCD. Because χ_{c1} is a P -wave state, the difference of dissociation temperature from J/Ψ and η_c is expected. As a result, we have observed the low-lying $c\bar{c}$ state much below the mass of χ_{c1} , $m_{\chi_{c1}} \simeq 3.5$ GeV. This state is identified as a scattering state through the analysis of the boundary-condition

dependence,

In this analysis, we have found no low-lying state corresponding to χ_{c1} above T_c in lattice QCD. Therefore, χ_{c1} already dissociates at $1.11T_c$.

For further analysis in χ_{c1} channel, we have also performed MEM analysis at $1.62T_c$ in lattice QCD with the Wilson quark action with $\beta = 7.0$ and $a_s/a_t = 4.0$. As a result, the spectral function has no peak structure corresponding to χ_{c1} around 3.5GeV. This fact also indicates that χ_{c1} already dissociate at $1.62T_c$.

Through the above analyses, we have observed the spatially localized bound state in high energy region, which is not affected by the spatial boundary condition at all. The bound state appearing in high-energy region on the lattice would be the bound state of doubler(s), which is unphysical.

Our study of charmonia indicates that the S -wave mesons J/Ψ and η_c survive even above T_c ($\sim 2T_c$) as compact bound states, while the P -wave meson χ_{c1} immediately dissociates above T_c .

We are performing the same analyses for other charmed mesons, e.g., D mesons. The narrowness of the decay width of charmonia strongly depends on whether the decay channel of $D\bar{D}$ opens or not. If the mass of the D meson is shifted at high temperature, a drastic change of decay width of some charmonia possibly occurs, which may be interesting both theoretically and experimentally.

The subject of hadrons in high density system is fascinating. For example, CERES collaboration presented interesting events on the lepton pair production in low-mass region from p-Be and p-Au (450GeV/c) and from S-Au (200GeV/c per nucleon) [36]. It is reported that the lepton pairs from S-Au in the invariant mass range $0.2\text{GeV}/c^2 < m < 1.5\text{GeV}/c^2$ are largely enhanced compared with the hadronic contributions, while those from p-Be and p-Au are not enhanced. The enhancement is considered to be the signal of the change of hadronic nature of vector mesons in finite density system [36, 37, 38]. Namely, the mass reduction and/or the width broadenings of vector mesons at finite density can lead to the enhancement of low-energy lepton pairs. At the experimental facility J-PARC in Japan, which is planned to run in 2008, the experiments of high density system are expected to take place. For these experiments, the theoretical study of finite density system is required. Then the study at finite density in lattice QCD is challenging and worth trying.

The survival of J/Ψ above T_c may change the scenario of J/Ψ suppression. These analyses give us the further knowledge of QCD at finite temperature.

Acknowledgments

We thank Prof. M. Oka for fruitful discussions and suggestions. H. S. and N. I. are supported in part by the Grant for Scientific Research [(B) No. 15340072 and (C) No. 16540236] from the Ministry of Education, Culture,

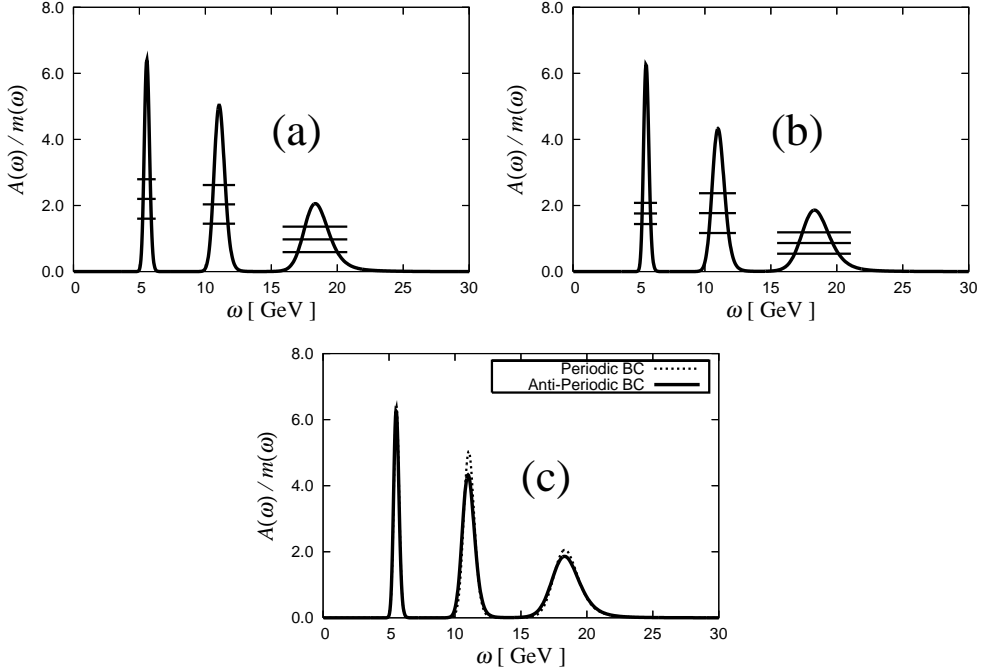


FIG. 11: The spectral function $A(\omega)$ of the $c\bar{c}$ state in axial vector ($J^P = 1^+$) channel on PBC (a) and APBC (b) at $1.62T_c$ extracted with MEM from lattice QCD data of the temporal correlator. $m(\omega)$ denotes the default model of MEM [23, 24, 25]. The statistical error is denoted by the three solid lines. There is no peak which corresponds to $\chi_{c1}(m_{\chi_{c1}} \simeq 3.5\text{GeV})$. The peaks in high-energy region ($\omega > 5\text{GeV}$) are considered as lattice artifacts. We add (c) as the comparison between PBC and APBC. These results almost coincide.

Sports, Science and Technology, Japan. H. I. is supported by the Japan Society for the Promotion of Science for Young Scientists. T. D. is supported by Special Postdoctoral Research Program of RIKEN. K. T. is supported

by a 21st Century COE Program at Kyoto University. Our lattice QCD calculations have been performed on NEC-SX5 at Osaka University.

[1] T. Celik, J. Engels and H. Satz, Phys. Lett. **B125**, 411 (1983).
[2] J.B. Kogut, M. Stone, H.W. Wyld, W.R. Gibbs, J. Shigemitsu, S.H. Shenker and D.K. Sinclair, Phys. Rev. Lett. **50**, 393 (1983).
[3] J.I. Kapusta, “Finite-temperature field theory”, Cambridge University Press (1989), and references therein.
[4] T. Hashimoto, O. Miyamura, K. Hirose and T. Kanki, Phys. Rev. Lett. **57**, 2123 (1986).
[5] T. Matsui and H. Satz, Phys. Lett. **B178**, 416 (1986).
[6] T. Hatsuda and T. Kunihiro, Phys. Rept. **247**, 221 (1994) and references therein.
[7] H. Ichie, H. Suganuma and H. Toki, Phys. Rev. D**52**, 2944 (1995); S. Sasaki, H. Suganuma and H. Toki, Phys. Lett. B**387**, 145 (1996).
[8] H. Iida, M. Oka and H. Suganuma, Eur. Phys. J. A**23**, 305 (2005).
[9] B.B. Back et al. [PHOBOS Collaboration], Nucl. Phys. A**757**, 28 (2005).
[10] I. Arsene et al. [BRAHMS Collaboration], Nucl. Phys. A**757**, 1 (2005).
[11] J. Adams et al. [STAR Collaboration], Nucl. Phys. A**757**, 102 (2005).
[12] K. Aderok et al. [PHENIX Collaboration], Nucl. Phys. A**757**, 184 (2005).
[13] M.C. Abreu et al. [NA50 Collaboration], Nucl. Phys. A**661**, 93c (1999); Phys. Lett. B**477**, 28 (2000).
[14] H.J. Rothe, “Lattice gauge theories (3rd edition)”, World Scientific (2005), and references therein.
[15] F. Karsch, J. Phys. G **30**, S887 (2004) and references therein.
[16] J. Rafelski and B. Müller, Phys. Rev. Lett. **48**, 416 (1982) [Erratum-ibid. **56**, (1986) 2334].
[17] S.S. Adler et al. [PHENIX Collaboration], Phys. Rev. Lett. **91**, 072303 (2003).
[18] X.N. Wang, Phys. Rept. **280**, 287 (1997).
[19] C. DeTar and J.B. Kogut, Phys. Rev. Lett. **59**, 399 (1987); Phys. Rev. D**36**, 2828 (1987).
[20] A. Nakamura and S. Sakai, Phys. Rev. Lett. **94**, 72305 (2005).
[21] T. Hirano and Y. Nara, Phys. Rev. Lett. **91**, 082301 (2003).
[22] T. Umeda, K. Katayama, O. Miyamura and H. Matsufuru, Int. J. Mod. Phys. A**16**, 2215 (2001); H. Matsufuru,

O. Miyamura, H. Saganuma and T. Umeda, AIP Conf. Proc. **CP594**, 258 (2001).

[23] M. Asakawa and T. Hatsuda, Phys. Rev. Lett. **92**, 012001 (2004).

[24] T. Umeda, K. Nomura and H. Matsufuru, Eur. Phys. J. **C39**, 9 (2005).

[25] S. Datta, F. Karsch, P. Petreczky, I. Wetzorke, Phys. Rev. **D69**, 094507 (2004) ; J. Phys. **G31**, S351 (2005).

[26] H. Iida, T. Doi, N. Ishii and H. Saganuma, PoS **LAT2005**, 184 (2005).

[27] N. Ishii, T. Doi, H. Iida, M. Oka, F. Okiharu and H. Saganuma, Phys. Rev. **D71**, 034001 (2005); N. Ishii, T. Doi, Y. Nemoto, M. Oka and H. Saganuma, Phys. Rev. **D72**, 074503 (2005).

[28] M. Lüscher, Nucl. Phys. **B354**, 531 (1991).

[29] N. Mathur, F.X. Lee, A. Alexandru, C. Bennhold, Y. Chen, S.J. Dong, T. Draper, I. Horvath, K.F. Liu, S. Tamhankar and J.B. Zhang, Phys. Rev. **D70**, 074508 (2004).

[30] T.T. Takahashi, T. Umeda, T. Onogi and T. Kunihiro, Phys. Rev. **D71**, 114509 (2005).

[31] T.R. Klassen, Nucl. Phys. **B533**, 557 (1998); H. Matsufuru, T. Onogi and T. Umeda, Phys. Rev. **D64**, 114503 (2001).

[32] N. Ishii, H. Saganuma and H. Matsufuru, Phys. Rev. **D66**, 094506 (2002); Phys. Rev. **D66**, 014507 (2002).

[33] A.X. El-Khadra, A.S. Kronfeld and P.B. Mackenzie, Phys. Rev. **D55**, 3933 (1997).

[34] T. Yamazaki, S. Aoki, R. Burkhalter, M. Fukugita, S. Hashimoto, N. Ishizuka, Y. Iwasaki, K. Kanaya, T. Kaneko, Y. Kuramashi, M. Okawa, Y. Taniguchi, A. Ukawa and T. Yoshie [CP-PACS Collaboration], Phys. Rev. **D65**, 014501 (2001).

[35] K. Tsumura et al., in preparation.

[36] G. Agakichiev et al. [CERES Collaboration], Phys. Rev. Lett. **75**, 1272 (1995).

[37] V.L. Eletsky, B.L. Ioffe and J.I. Kapusta, Eur. Phys. J. **A3**, 381 (1998); V.L. Eletsky, B.L. Ioffe, Phys. Rev. Lett. **78**, 1010 (1997); Phys. Lett. **B477**, 28 (2000).

[38] H. Iida, M. Oka and H. Saganuma, Nucl. Phys. **B141** (Proc. Suppl.), 191 (2005).